ARTICLES

Journal of Semiconductors
(2023) 44, 032801
doi: 10.1088/1674-4926/44/3/032801

Investigation of UV photosensor properties of Al-doped SnO_2 thin films deposited by sol-gel dip-coating method

Kaour Selma[1, 2], Benkara Salima[3, 4, †], Bouabida Seddik[3], Rechem Djamil[1, 3], and Hadjeris Lazhar[1, 2]

[1]Laboratory of Materials and Structure of Electromechanical Systems and their Reliability, Oum El Bouaghi University, Algeria

[2]Faculty of Exact Sciences and Natural and Life Sciences, Oum El Bouaghi University, Algeria

[3]Electrical Engineering Department, Oum El Bouaghi University, Algeria

[4]Laboratory of Active Components and Materials, Oum El Bouaghi University, Algeria

Abstract: Transparent conducting aluminum doped tin oxide thin films were prepared by sol-gel dip coating method with different Al concentrations and characterized by X-ray diffraction (XRD), atomic force microscopy (AFM), UV–Vis spectrophotometry and photoconductivity study. The variation observed in the properties of the measured films agrees with a difference in the film's thickness, which decreases when Al concentration augments. X-ray diffraction analysis reveals that all films are polycrystalline with tetragonal structure, (110) plane being the strongest diffraction peak. The crystallite size calculated by the Debye Scherrer's formula decreases from 11.92 to 8.54 nm when Al concentration increases from 0 to 5 wt.%. AFM images showed grains uniformly distributed in the deposited films. An average transmittance greater than 80% was measured for the films and an energy gap value of about 3.9 eV was deduced from the optical analysis. Finally, the photosensitivity properties like current–voltage characteristics, I_{ON}/I_{OFF} ratio, growth and decay time are studied and reported. Also, we have calculated the trap depth energy using the decay portion of the rise and decay curve photocurrent.

Key words: tin oxide; thin films; sol-gel; UV photodetector; photoconductivity; trap depth

Citation: K Selma, B Salima, B Seddik, R Djamil, and H Lazhar, Investigation of UV photosensor properties of Al-doped SnO_2 thin films deposited by sol-gel dip-coating method[J]. *J. Semicond.*, 2023, 44(3), 032801. https://doi.org/10.1088/1674-4926/44/3/032801

1. Introduction

UV photodetectors have attracted considerable attention in recent years due to their application in environmental, biological analysis, optical communication, flam detection, astronomy lithography and detection of missiles[1, 2]. Transparent conductive oxide (TCO) films such as tin oxide (SnO_2), zinc oxide (ZnO) and titanium oxide (TiO_2) are frequently utilized for the UV photodetectors application[3–6]. In particular, most attention concerned tin oxide (SnO_2) semiconductor due to its special properties, which made it a required material for optical and optoelectronic applications[7, 8] such as wide band gap (3.6–4 eV)[9, 10], large exciton binding energy (about 131 eV)[11], high optical transmittance[12], chemical stability and n-type character due to native defects such as oxygen vacancies and tin interstitials, which can exist in two possible valence states: Sn^{2+} and Sn^{4+}[13]. A notable defect in SnO_2 and most metal oxides are oxygen vacancies[14]. These defects may behave like traps for free electrons or holes, such as a recombination or generation center, which strongly influence the photoconductivity and photoresponse process[15]. However, persistent photoconductivity and big recovery times are problematic characteristics due to deep traps[16]. Information about these traps levels can be obtained from the decay curve of photoconductivity after cutoff of excitation[17, 18].

Previous studies[19–22] demonstrated that the control of the concentration of oxygen vacancy by doping with different elements such as magnesium[19], nickel[20], tin[21] and aluminum[22–24] is among the ways to improve the performance of UV photodetectors in metal oxides[25, 26]. The doping process such Al, change the type of SnO_2 from n to p by substitution of Sn^{4+} by Al^{3+} ion and causing a disorder and some scattering centers, resulting in an increase in hole concentration with increasing the Al content[27, 28]. Also, the method and conditions of synthesis have a basic role in UV photodetectors properties such as solution concentration[25], thin film thickness[26], annealing temperature and time, the photoresponse being profoundly augmented with increasing annealing time[29].

Elaboration conditions have a big influence on the properties and qualities of layers. SnO_2 thin films can be obtained by numerous methods of deposition[30–33], among them, sol-gel dip coating technique presents several advantages such as simplicity, excellent homogeneity, the possibility of ease doping, low cost, large area substrate coatingand low reaction temperature. Moreover, Al-doped SnO_2 thin films can be obtained easily using this technique, which makes them very attractive in many applications such as gas sensors[34] and solar cells[35]. The thin films photoconductivity properties based on pure and doped SnO_2 have been studied by a number of research such as Sb-doped SnO_2[36], As-doped SnO_2[37], Al-doped SnO_2[38], and the effect of twin boundaries on photocurrent decay of the pure SnO_2[39]. However, the studies about

Correspondence to: B Salima, sali_benkara@yahoo.fr
Received 10 SEPTEMBER 2022; Revised 5 NOVEMBER 2022.

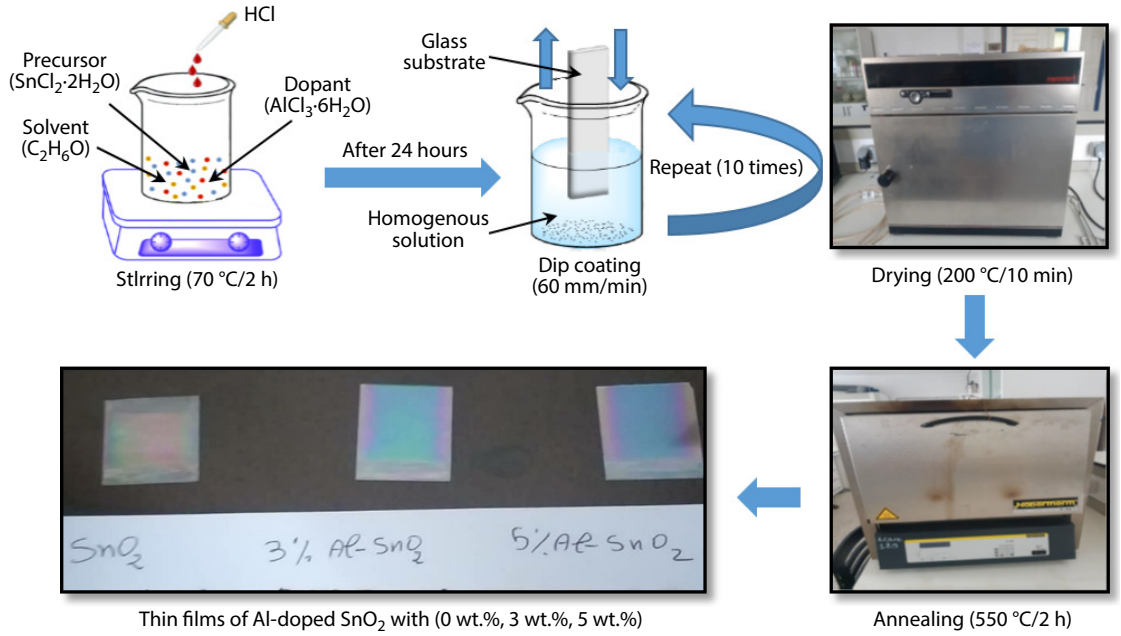

Fig. 1. (Color online) The schematic drawing of pure and Al-doped SnO_2 thin films produced with a sol-gel dip coating method.

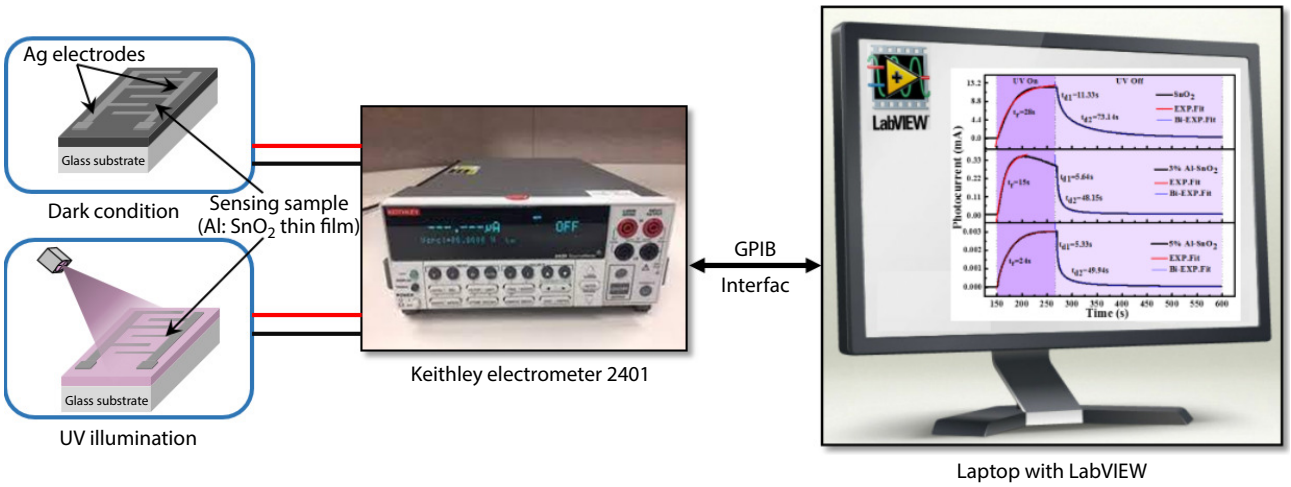

Fig. 2. (Color online) Experimental setup of UV photo-detection.

the UV photoconductivity and photosensitivity in Al-doped SnO_2 thin films prepared by sol-gel dip coating are not enough.

In this work, we prepared Al-doped SnO_2, using sol-gel process. The influence of aluminum concentration on the performance of UV photodetectors based on SnO_2 thin films had been studied.

2. Experimental details

2.1. Samples preparation and characterization

Using a sol-gel dip coating method, undoped and aluminum doped SnO_2 thin films were successfully deposited on glass substrates. Tin (II) chloride ($SnCl_2·2H_2O$) was dissolved in 30 mL of ethanol absolute (C_2H_6O), then a few drops of HCl were added to the solution for accelerating the hydrolysis reaction between the precursor and the solvent. Aluminum trichloridehexahydrate ($AlCl_3·6H_2O$), was added to the solution for Al doping (3 wt.%, and 5 wt.%). After vigorously stirring at 70 °C for 120 min, we obtained a homogenous solution. On the other hand, the glass substrate was cleaned with acetone, ethanol and deionized water for 10 min in the ultrasonic bath and then dried at room temperature. The substrates were immersed in the solution for 1 min with a withdrawal speed of 60 mm/min, and next dried at 200 °C for 10 min. After repeating this procedure 10 times, the films were annealed at 550 °C for 2 h. Fig. 1 shows the process of synthesizing pure and Al-doped SnO_2 thin films using the sol-gel process.

X-ray diffraction (XRD, Burker AXS-8D) with CuKα (λ = 1.541 Å) radiation was used to study the structural properties. The surface morphology of the SnO_2 films was performed by atomic force microscopy (A100-AFM). UV-visible spectrophotometer (JascoV-360) was used to study the optical properties in the range (200–1100 nm) to determine the band gap of samples.

2.2. Photodetectors measurements

Pure and Al-doped SnO_2 based UV photodetection measurements were performed using Ag electrodes in a planar interdigital configuration as shown in Fig. 2. The Keithley (2401) source meter was used to measure the current–voltage (I–V) characteristics in dark and under UV illu-

Table 1. XRD parameters, crystallite size, strain and RMS of undoped and Al-doped SnO_2 thin films.

Sample	2θ (°)	B (°)	D (nm)	Strain (10^{-3})	$a = b$ (Å)	c (Å)	RMS (nm)	R_a (nm)	D_a (nm)
SnO_2	26.79	0.71	11.92	3.27	4.700	3.203	5.06	4.25	73.0
3 wt.% Al-SnO_2	26.56	0.74	11.40	3.42	4.742	3.195	2.32	1.76	45.5
5 wt.% Al-SnO_2	26.58	0.99	08.54	4.60	4.738	3.161	2.01	1.67	29.3

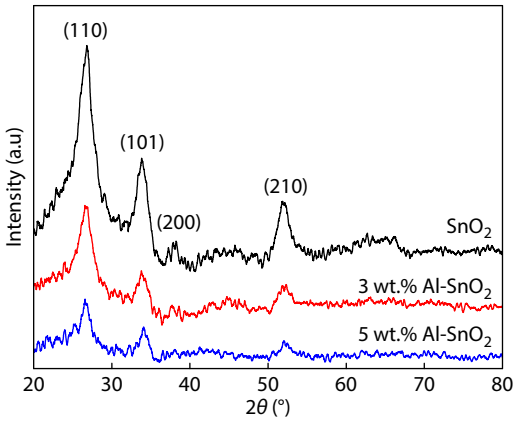

Fig. 3. (Color online) XRD patterns of undoped and Al-doped SnO_2 thin films.

mination to determine the UV photoresponse. Illumination was performed by a UV lamp (VL-4LC, vilberlourmat) available in two wavelengths: 254 and 365 nm, and an intensity of 350 μW/cm^2.

3. Result and discussion

3.1. X-ray diffraction studies

X-ray diffraction patterns for undoped and Al-doped SnO_2 thin films are shown in Fig. 3. These films exhibit a polycrystalline nature in a tetragonal rutile structure (JCPDS 41-1445). No peaks related to Al or Al_2O_3 were detected in the XRD pattern this may be caused to the low Al content and the Al^{3+} ions have been replaced by Sn^{4+} site without changing tetragonal structure[40]. In previous studies, the SnO_2 thin films doped with Al and prepared by sol-gel don't detect secondary phases related to Al doping[41]. It can be seen that the (110) plane is the strongest diffraction peak. Other less-intense peaks are observed at (101), (200) and (210) planes. In addition, the intensity of the diffraction peaks decreases with increasing Al concentration, the augmentation of which reduces the film thickness. These results indicate to uniform distribution of Al ions across the SnO_2 lattice[42] and agree with some reports[41, 43].

The crystallite size (D) can be calculated from the Scherrer's equation[7]:

$$D = \frac{K\lambda}{\beta\cos\theta}, \tag{1}$$

where K is a constant (shape factor, about 0.9), λ is the X-ray wavelength, β is the full width at half maximum of the XRD peak, θ is the Bragg diffraction angle.

The (110) peak was utilized to estimate the crystallite size. It can be noticed from Table 1 that the crystallite size of the films decreases from 11.92 to 8.54 nm when Al concentration increases from 0 to 5 wt.% concentration. This proves that the incorporation of Al^{3+} into SnO_2 structure obstructs crystallization and prevents crystal growth[44].

To calculate the lattice parameters $a = b$ and c, the following equations have been used[45]:

$$\frac{1}{d_{hkl}^2} = \frac{h^2 + k^2}{a^2} + \frac{l^2}{c^2}, \tag{2}$$

$$a = b = \sqrt{2}d_{(hkl)} = \sqrt{2}d_{(110)}, \tag{3}$$

$$c = \frac{1}{\sqrt{\frac{1}{d_{(101)}^2} - \frac{1}{a^2}}}. \tag{4}$$

From Table 1, the lattice parameters and unit cell volume of deposited SnO_2 thin films correspond with the perfect values $a = b = 4.738$ Å, $c = 3.186$ Å and $V = 71.5$ Å. Furthermore, the lattice parameter increases from 4.70 to 4.742 Å when Al concentration increases from 0 to 3 wt.% and then decreases to 4.738 Å when Al concentration is equal to 5 wt.%. This change in a random manner in lattice parameters a and b may be due to a disturbance in the grains of the film after doping with Aluminum[46].

Moreover, the strain (ε) of the films was estimated using the following relation[40]:

$$\varepsilon = \frac{\beta\cos\theta}{4}. \tag{5}$$

The change of strain in the SnO_2 thin films observed in Table 1 can be explained by the variation in dopant concentration. The strain increases with increasing Al concentration because the incorporation, into the SnO_2 lattice of Al, which has an ionic radius (0.53 Å) smaller than Sn (0.69 Å), leads to defects and lattice distortions, resulting in a different type of stress. The mean crystallite size is estimated to be ~ 11.92 nm for the undoped sample and it shows a decreasing tendency as the Al content is increased. This behavior can be attributed to the change in lattice parameters[47] and the increase of strain in the thin films that affect the normal growth of SnO_2, these results generally agree with the changes observed in the lattice parameters. Related results have been noted in the literature for Ni-doped SnO_2[48] and Ti-doped SnO_2[47]. The solubility of dopants is basically dependent on valence state and ionic radius value.

The calculation of the texture coefficient $T_c(hkl)$ allows us to deduce the preferred orientation of growth via the following formula[46]:

$$T_c(hkl) = \frac{I_{(hkl)}/I_{0(hkl)}}{\frac{1}{n}\left(\sum I_{(hkl)}/I_{0(hkl)}\right)}, \tag{6}$$

where $I_{(hkl)}$ is the measured intensity of the (hkl) peak, $I_{0(hkl)}$ is the standard intensity of (hkl) peak corresponding to the JCPDS data and n is the diffraction peaks observed.

Table 2. The values of Texture Coefficient of undopedand Al-doped SnO_2 thin films.

Sample	$T_c(hkl)$ of SnO_2 thin films			
	(110)	(101)	(200)	(210)
SnO_2	1.22	1.17	0.78	0.83
3 wt.% Al-SnO_2	1.41	0.94	0.86	0.77
5 wt.% Al-SnO_2	1.33	1.12	0.62	0.91

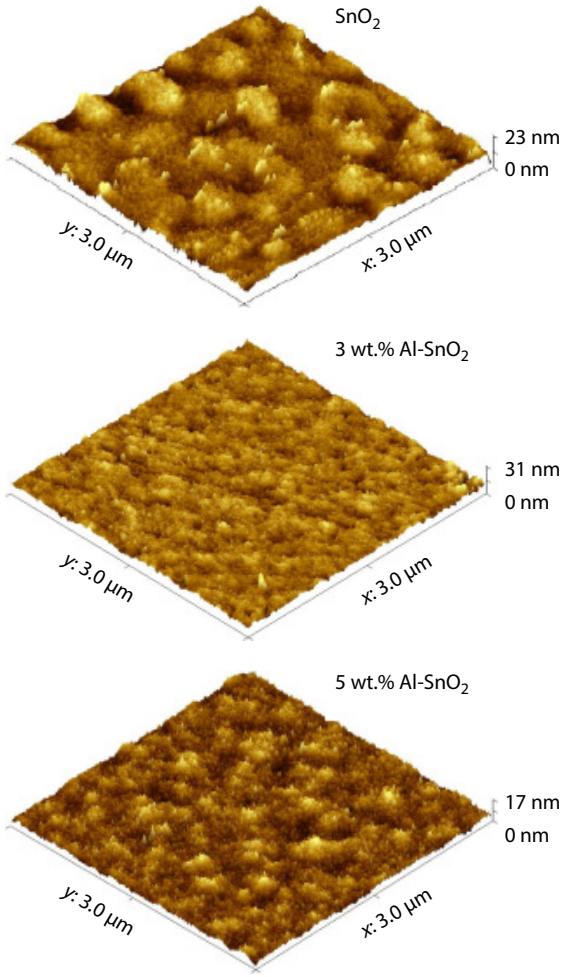

Fig. 4. (Color online) 3D surface morphologies of SnO_2 thin films with various Al doping concentrations.

Table 2 shows the texture coefficient values for (110), (101), (200) and (210) peaks. The (110) diffraction peak presented a high texture coefficient value for all deposited films, which means the (110) plan is the preferred orientation, this confirmed the XRD patterns results. The origin of preferential orientation along (110) can be interpreted by the periodic bond chain (PBC) theory[46]. Via this theory, the SnO_2 crystals faces can be divided into flat (F), stepped (S) and kinked (K) according to 2, 1 and none number respectively of PBC parallel to the faces (*hkl*). Forms F and K are of great interest for cassiterite of SnO_2. Since they consist of (101) and (111) crystal planes, respectively[49]. For the crystal grains formed by (101) F faces are two possible preferred orientations, namely (110) and (001). Since the (001) orientation was not observed by XRD, the (110) preferential orientation was formed by the (101) F faces[50]. These results are similar to some previous reports[51].

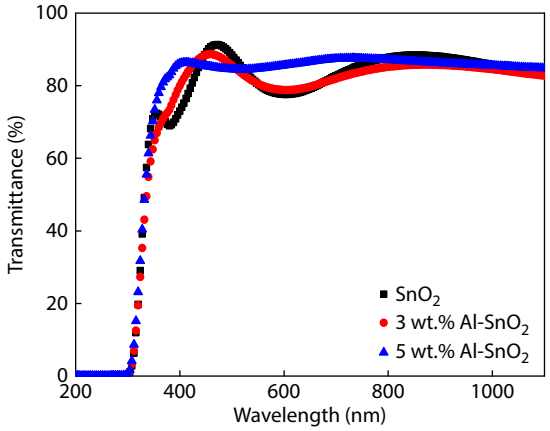

Fig. 5. (Color online) Optical transmittance spectra of undoped and Al-doped SnO_2 thin films.

3.2. Surface morphological study

For analyzing the surface morphology of SnO_2 thin films doped with different Al doping concentrations, the atomic force microscope was used. The area of 3 × 3 μm^2 was scanned. From 3D AFM images, which are obtained by high scan mode and illustrated in Fig. 4. It can be clearly seen that the surface morphology of pure film is very different from Al-doped SnO_2 thin films.

The values of the root mean square roughness (RMS), the average roughness (R_a) and the grain size (D_a) for all films were evaluated using Gwyddion 2.60 program and reported in Table 1. It can be noted that the surface roughness is strongly dependent on the Al concentration. The values of RMS and R_a decreases from 5.06 to 2.01 nm and from 4.25 to 1.67 nm when Al concentration increases from 0 to 5 wt.%. The low values of RMS and R_a for prepared films are similar to the result which has been obtained from the In-doped SnO_2 thin films deposited with sol-gel spin coating technique[52] and from Zr-doped SnO_2 thin films synthesized by spray pyrolysis[53]. As for grain size, it also decreases with the increase in Al^{+3} ions concentration and it is in good agreement with the XRD results. As well, the size of the grains estimated from AFM is bigger than that determined through XRD. This is due to the fact that AFM reveals particle agglomerations, whereas XRD provides an average grain size[53].

3.3. Optical study

The optical transmission spectra of undoped and Al-doped tin oxide thin films elaborated by sol-gel dip coating technique on a glass substrate and annealed at 550 °C are plotted in Fig. 5. All films display high transmittance greater than 80% in the 400–1100 nm interval of wavelength. According to Ref. [54], the low transmittance for Sn-doped films may be due to the increased optical scattering caused by the rough surface morphology.

From the observation of interference fringes, one can deduce that the film thickness decreases as Al concentration augments. The band gap energy values of Al-doped tin oxide thin films were calculated by using the Tauc equation[55]:

$$\alpha h\upsilon = A\left(h\upsilon - E_g\right)^{1/2}, \tag{7}$$

where α is the absorption coefficient, A is constant, $h\upsilon$ is photon energy and E_g is the band gap energy. The results are

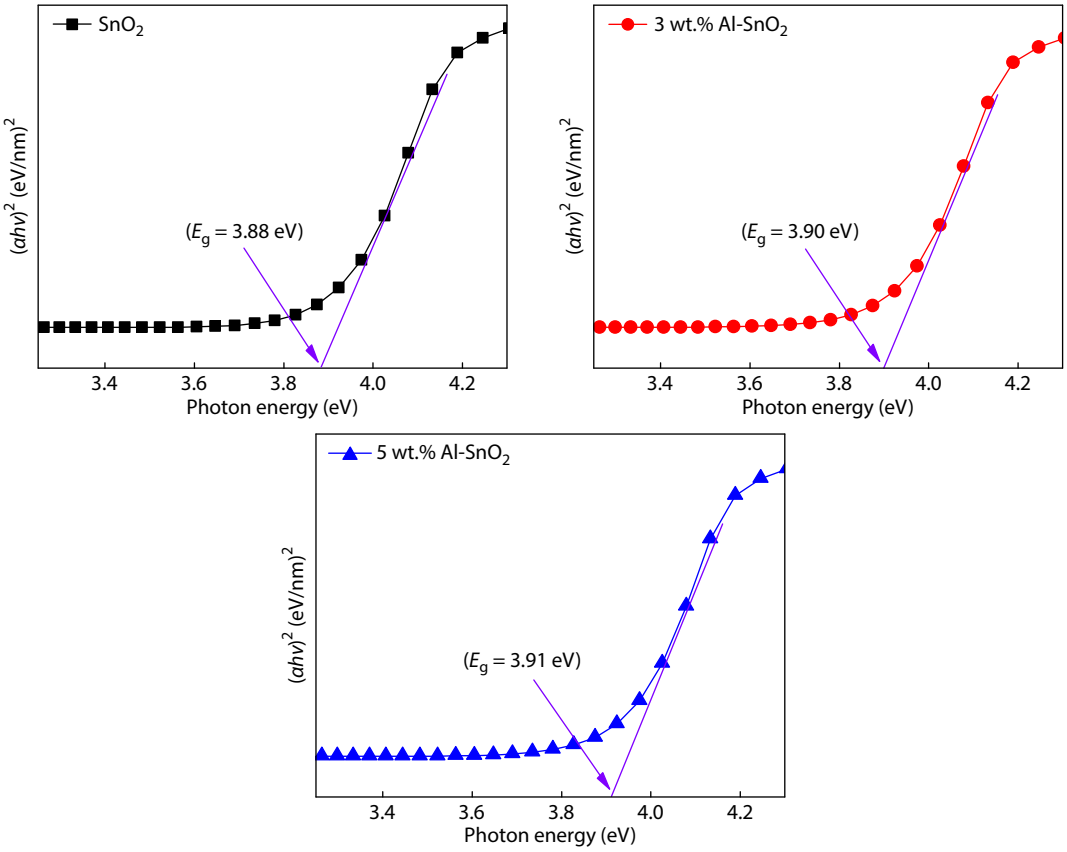

Fig. 6. (Color online) Plots $(ahu)^2$ versus hu of undoped and Al-doped SnO_2 thin films.

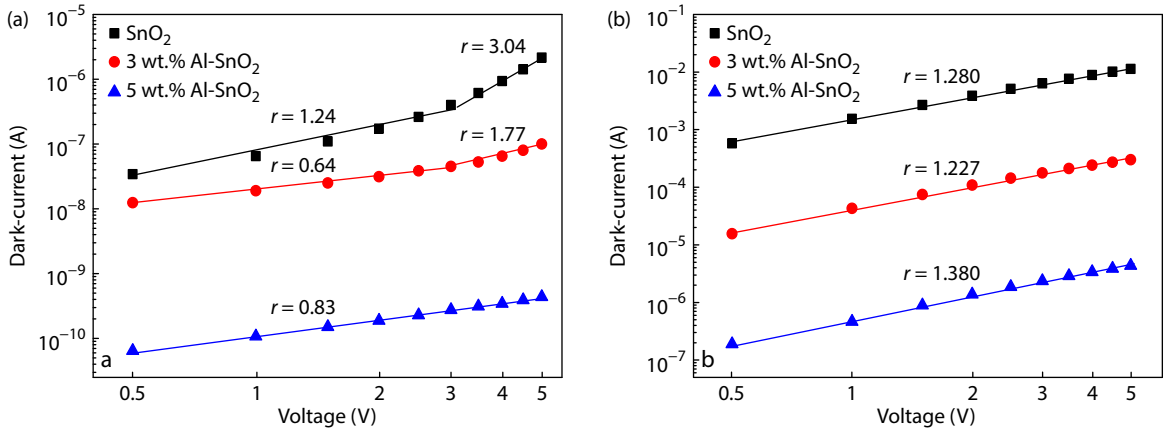

Fig. 7. (Color online) Variation of (a) dark current and (b) photocurrent as a function of applied voltage for undoped and aluminum doped SnO_2 thin films.

shown in Fig. 6. The band gap value increases from 3.88 to 3.91 eV when Al concentration increases from 0 to 5 wt.%. Similar results have been reported by Ahmed[41] and Baghri-Mohagheghi[56]. The increase in gap energy after adding Al with 3 wt.% and 5 wt.% ratio may be due to a reduction in particle size and Burstein-Moos effect[57].

3.4. Photosensor study

3.4.1. Effect of voltage on photocurrent

Variation of photo and dark current with a voltage of undoped and Al-doped SnO_2 thin films in log-log scale as shown in Fig. 7. It can be noticed that the curves are straight lines having a different slope with regard to different voltage according to the power law relation $I \propto V^r$, where r is the slope of different straight line segments[18, 29]. In the absence of illumination (Fig. 7(a)), the log-log plot of I–V characteristics of pure and the sample doped with 3 wt.% aluminum can be divided into two separate regions. For pure SnO_2, the dark current varies super linearly ($r = 1.24$) at a voltage below 3.5 V. Above 3.5 V, it can show space charge limited current (SCLC) behavior ($r = 3.04$). It is significant that at the high voltage the dark current for undoped SnO_2 thin films engenders from space charge of excess carriers injected from one of the electrodes and the traps of materials also contribute to this behavior[58, 59]. The SCLC phenomena is reported by Aldemir *et al.* for photodiode based on Al-doped SnO_2 thin films prepared using spray pyrolysis[38]. However, sub-linearly variation ($r = 0.64$) at the voltage below 3.5 V varies to super linearly variation ($r = 1.77$) at the voltage above 3.5 V is recorded with the sample doped with 3 wt.% of aluminum, the

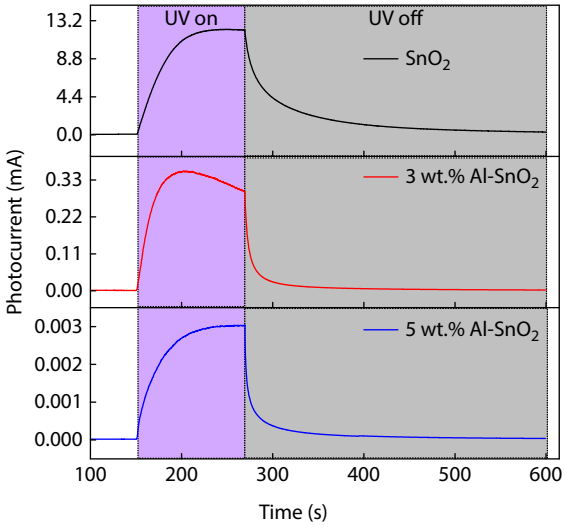

Fig. 8. (Color online) Photoconductivity rise and decay time spectra of undoped and Al-doped SnO_2 thin films.

flow of trap limited and space charge limited current inside the material is responsible for this type of variation[58, 17]. The dark current for the sample doped with 5 wt.% Al varies sublinearly (r = 0.83 < 1), the sublinear variation with applied voltage in this sample could be because of the emergence of blocking contacts that do not entirely refill the charge carriers after they are captured by electrodes[58, 60].

The dependence of photocurrent with applied voltage in Fig. 7(b) shows super-linear behavior for all samples, the super-linear behavior of the dark current and photocurrent may be due to additional charge carriers being injected from one of the electrodes[61].

3.4.2. Rise and decay photocurrent

Fig. 8 shows the photoconductivity rise and decay time spectra of undoped and Al-doped SnO_2 thin films. The measurements were obtained under 5 V bias voltages and UV light lamp with wavelength 365 nm at room temperature. One observation we can remark, the dark current (I_{OFF}) and photocurrent (I_{ON}) decrease with increased Al ions concentration. Furthermore, for pure and 5 wt.% Al-SnO_2 samples, when the light is turned on, the current increased quickly in the beginning, then it continues to slowly increase until the UV light is turned off again. As for 3 wt.% Al-SnO_2 sample, when the UV illumination is turned on, the current begins to increase until it reaches maximum value, then it decreases until the UV radiation turned off. The anomalous photocurrent behavior for 3 wt.% Al-SnO_2 may be due to the recombination of photo generation carriers[62]. Similar retreat photoconductivity behavior was reported for SnO_2 nanoparticles that have been synthesized using the chemical co-precipitation method[62] and for 4 wt.% In-doped ZnO sol-gel spin coated film[63]. Another hand, when UV illumination was turned off, the current initially decrease very fast, later it continues to decrease gradually; the persistence effect photoconductivity phenomenon was reduced with the samples doped with aluminum.

In order to more explain, it is necessary to understand the mechanism of UV photoconductivity response in pure and Al-doped SnO_2 thin films. Fig. 9 schematizes the mechanism of UV photoconductivity for SnO_2 thin films. In the dark current, the molecules of oxygen O_2 (g) are stuck in the surface of thin films with an adsorption process by capturing free electrons; this produces a depletion region near the surface[63], which leads to a decrease in the current at the surface of Al-SnO_2 thin films[64]. The following reaction exemplifies this process.

$$O_2\,(g) + e^- \rightarrow O_2^-. \tag{8}$$

In the light condition, the electron–hole pairs produced by absorption of photon have at least equal energy as the band gap of Al-SnO_2 thin films. Moreover, the oxygen ions O_2^- will recombine with the generated holes to be chemisorbed from the surface. This reduces the depletion layer near the surface of SnO_2 thin films and it allows to the photo generatedelectron and the free electron that generated by chemisorbed step migrate to conduction band and contributed in photosensitivity process when applying the bias voltage[65].

$$h\nu \rightarrow e^- + h^+, \tag{9}$$

$$O_2^- + h^+ \rightarrow O_2\,(g). \tag{10}$$

After returning to the dark again, the photocurrent decrease, due to recombination of the (e–h) pairs which was generated by absorption process and the repetition adsorption of oxygen[66].

The sensitivity (S) or I_{ON}/I_{OFF} ratio is an important parameter for describing the performance of photodetectors. The film of 3 wt.% Al-SnO_2 shows the highest value of sensitivity and it was estimated at 273.85, while for the film 5 wt.% Al-SnO_2 decreased to 151.38.

Other parameters play a crucial role in the photodetector as the rise and decay time. Fig. 10 shows that using the exponential and Bi-exponential functions, the rise and decay time are approximated by the fitting curve.

$$I_{ph} = I_0 + A_1 e^{-t/t_r}, \tag{11}$$

$$I_{ph} = I_{ph(\infty)} + A_2 e^{-t/t_{d1}} + A_3 e^{-t/t_{d2}}, \tag{12}$$

where I_0 is the dark current, A_1, A_2, A_3 are constants, t_r is the rise time and t_{d1} and t_{d2} are the decay time constants respectively for a fast and a slow decrease of photocurrent. The fast decrease was attributed to recombination of photogenerated electron–hole pairs process, whereas the slow decrease was attributed to readsorption process[67].

Table 3 shows the values of constant times for our films and other references. The 3 wt.% Al-SnO_2 shows the best rise and decay time constants values. There is improvement in the photoconductivity parameters as rise time, decay time and I_{ON}/I_{OFF} ratio for our films compare to previous values presented in the literature[39, 68, 69].

3.4.3. Trap depth study

Electron trap depth is calculated using the decay portion of the rise and decay curve when the current of decay is expressed by the bub model[3, 70]:

$$I = I_0 e^{(-Pt)}, \tag{13}$$

where I_0 is the current when the light is turned off, I is the pho-

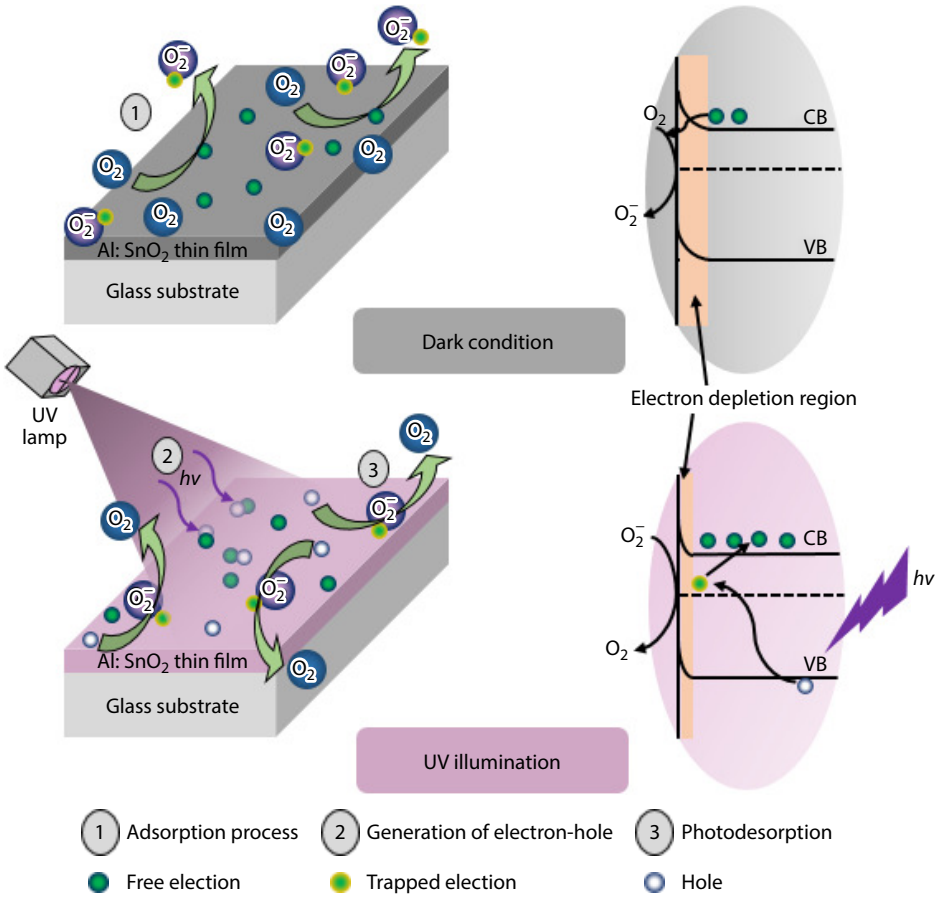

Fig. 9. (Color online) A schematic of the photoresponse mechanism and energy band diagram of Al:SnO_2 thin films.

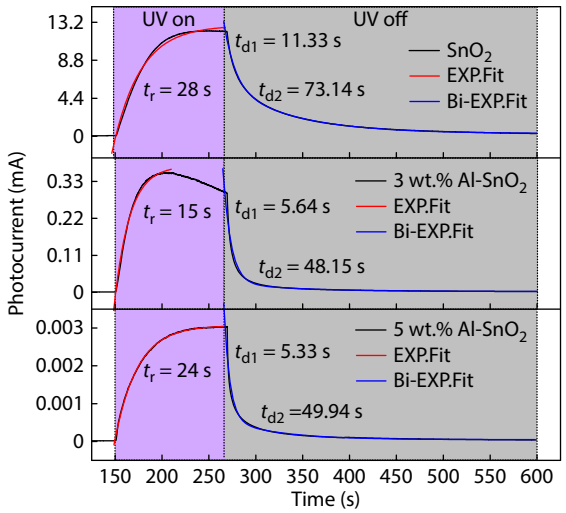

Fig. 10. (Color online) Rise and decay photoresponse curves of pure and Al-doped SnO_2 thin films.

tocurrent versus time and P is the probability of escape of an electron from the trap persecond. The probability of an electron escaping from a trap has been described by Randal and Wilkins as[71]:

$$P = Se^{-E/K_BT}, \tag{14}$$

where T is the absolute temperature, K_B is the Boltzmann constant and S is the attempt to escape frequency (equal to 109 at room temperature).

The trap depth corresponding to different exponentials can be calculated by using the below equation[18].

$$E = K_BT\left(\ln S - \ln\frac{\ln I_0/I}{t}\right). \tag{15}$$

The values of trap depths (E) for undoped and Al-doped SnO_2 are listed in Table 3. The changes in the trap depth values reveal the defect and disorder that occurs in thin films structure. For our deposited films, trap depth energy decreases with an increase in Al ratio from 0 to 5 wt.%, this indicates that the stability and idealism of crystalline structure decrease with increased Al concentration[72], and leads to a reduction in the energy required to eliminate an electron from trap level[73]. It is confirmed by XRD results, as the strain values increase with increasing Al concentration. The values of traps depth calculated for our deposited films is between 0.579 and 0.640 eV which is greater than the previous reported values for Europium doped SnO_2 nanoparticles prepared by the co-precipitation method which is 0.33 and 0.35 eV[74], furthermore, our obtained values are very convergent to the taps depth values of ZnO thin films elaborated by sol-gel spin-coating technique[61].

4. Conclusions

In the present work, we have studied the photoconductivity and defect levels in undoped and Al-doped SnO_2 thin films elaborated using low-cost sol-gel method. Films properties were investigated by X-ray diffraction (XRD), Atomic force microscopy (AFM) and UV-visible spectrophotometry. Presented results demonstrated that our samples show a polycrystalline tetragonal rutile structure and high homogenous surface; moreover, prepared films show high transparency in a visible wavelength region with an average transmittance

Table 3. The values of photocurrent, dark current, I_{ON}/I_{OFF} ratio, rise time constant (t_r), decay time constants (t_{d1}, t_{d2}) and defect levels energy (trap depth (E_1, E_2)) for undoped and Al-doped SnO_2 thin films.

Sample	I_{ON} (A)	I_{OFF} (A)	I_{ON}/I_{OFF}	t_r (s)	t_{d1} (s)	t_{d2} (s)	E_1 (eV)	E_2 (eV)	Ref.
SnO_2	1.22×10^{-2}	7.75×10^{-5}	217.85	28	11.33	73.14	0.598	0.64	This work
3 wt.% Al-SnO_2	3.56×10^{-4}	1.30×10^{-6}	273.84	15	5.64	48.15	0.580	0.63	This work
5 wt.% Al-SnO_2	3.03×10^{-6}	1.95×10^{-8}	155.38	24	5.33	49.94	0.579	0.63	This work
Mg-ZnO films	–	–	8.49	196	14.3	112.1	0.640	0.70	[68]
Cu/LiZnO	9.6×10^{-11}	1.20×10^{-7}	1250	769	35	222	–	–	[69]
SnO_2 films	3.2×10^{-11}	1.43×10^{-9}	44	250	506	–	–	–	[39]

between 80% and 90%. For photo-detection studies, 3 wt.% Al-doped SnO_2sample shows the highest I_{ON}/I_{OFF} ratio and the best rise and decay time parameters. The photoconductivity mechanism was interpreted by adsorption and desorption phenomena and the defect energy levels were calculated using the decay portion curve of photoconductivity spectra.

Through this study, we reached the possibility of fabrication of a UV photodetector with high sensitivity, fast response and good physical properties based on 3 wt.% Al-doped SnO_2 thin films using the sol-gel dip-coating technique.

Acknowledgements

The authors appreciate the support of the laboratory of active components and materials, Oum El Bouaghi University. Authors also express sincere thanks to the crystallography laboratory of Constantine University for XRD measurements.

References

[1] Al-Zuhairi O, Shuhaimi A, Nayan N, et al. Non-polar gallium nitride for photodetection applications: A systematic review. Coatings, 2022, 12, 275

[2] İlhan M, Koc M M, Coskun B, et al. Structural and optoelectronic characterization of Cu_2CoSnS_4 quaternary functional photodetectors. Optik, 2020, 212, 164724

[3] Mishra S K, Bayan S, Shankar R, et al. Efficient UV photosensitive and photoluminescence properties of sol-gel derived Sn doped ZnO nanostructures. Sens Actuat A, 2014, 211, 8

[4] Liu H Y, Lin W X, Sun W Q, et al. A study of ultrasonic spray pyrolysis deposited rutile-TiO_2-based metal-semiconductor-metal ultraviolet photodetector. Mater Sci Semicond Process, 2017, 57, 90

[5] Khayatian A, Kashi M A, Azimrad R, et al. Effect of annealing process in tuning of defects in ZnO nanorods and their application in UV photodetectors. Optik, 2016, 127, 4675

[6] Oshima T, Okuno T, Fujita S. UV-B sensor based on a SnO_2 thin film. Jpn J Appl Phys, 2009, 48, 120207

[7] Leem J W, Yu J S. Physical properties of electrically conductive Sb-doped SnO_2 transparent electrodes by thermal annealing dependent structural changes for photovoltaic applications. Mater Sci Eng B, 2011, 176, 1207

[8] Song P, Wang Q, Yang Z X. Preparation, characterization and acetone sensing properties of Ce-doped SnO_2 hollow spheres. Sens Actuat B, 2012, 173, 839

[9] Khan A F, Mehmood M, Aslam M, et al. Characteristics of electron beam evaporated nanocrystalline SnO_2 thin films annealed in air. Appl Surf Sci, 2010, 256, 2252

[10] Kumari N, Ghosh A, Tewari S, et al. Synthesis, structural and optical properties of Al doped SnO_2 nanoparticles. Indian J Phys, 2014, 88, 65

[11] Sivasankar Reddy A, Figueiredo N M, Cavaleiro A. Nanocrystalline Au:Ag:SnO_2 films prepared by pulsed magnetron sputtering. J Phys Chem Solids, 2013, 74, 825

[12] Dien E, Laurent J M, Smith A, et al. Comparison of optical and electrical characteristics of SnO_2-based thin films deposited by pyrosol from different tin precursors. J Eur Ceram Soc, 1999, 19, 787

[13] Tran Q P, Fang J S, Chin T S. Optical properties and boron doping-induced conduction-type change in SnO_2 thin films. J Electron Mater, 2016, 45, 349

[14] Bonu V, Das A, Amirthapandian S, et al. Photoluminescence of oxygen vacancies and hydroxyl group surface functionalized SnO_2 nanoparticles. Phys Chem Chem Phys, 2015, 17, 9794

[15] Moazzami K, Murphy T E, Phillips J D, et al. Sub-bandgap photoconductivity in ZnO epilayers and extraction of trap density spectra. Semicond Sci Technol, 2006, 21, 717

[16] Brinzari V. Mechanism of band gap persistent photoconductivity (PPC) in SnO_2 nanoscrystalline films: Nature of local states, simulation of PPC and comparison with experiment. Appl Surf Sci, 2017, 411, 437

[17] Mishra S K, Srivastava S, Srivastava R K, et al. Photoluminescence and ultraviolet photoresponse in ZnO nanophorsphors prepared by thermal decomposition of zinc acetate. Adv Mater Lett, 2011, 2, 298

[18] Mishra S K, Srivastava R K, Prakash S G, et al. Photoluminescence and photoconductive characteristics of hydrothermally synthesized ZnO nanoparticles. Opto-Electron Rev, 2010, 18, 467

[19] Ku C J, Reyes P, Duan Z Q, et al. $Mg_xZn_{1-x}O$ thin-film transistor-based UV photodetectorwith enhanced photoresponse. J Electron Mater, 2015, 44, 3471

[20] Huang S Y, Matsubara K, Cheng J, et al. Highly enhanced ultraviolet photosensitivity and recovery speed in electrospun Ni-doped SnO_2 nanobelts. Appl Phys Lett, 2013, 103, 141108

[21] Kumar M, Bhatt V, Abhyankar A C, et al. Modulation of structural properties of Sn doped ZnO for UV photoconductors. Sens Actuat A, 2018, 270, 118

[22] Akin N, Baskose U C, Kinaci B, et al. AZO thin film-based UV sensors: Effects of RF power on the films. Appl Phys A, 2015, 119, 965

[23] Singh S. Simulation, fabrication, and characterization of Al-doped ZnO-based ultraviolet photodetectors. J Electron Mater, 2016, 45, 535

[24] Mahroug A, Boudjadar S, Hamritet S, al. Structural, optical and photocurrent properties of undoped and Al-doped ZnO thin films deposited by sol-gel spin coating technique. Mater Lett, 2014, 134, 248

[25] Inamdar S I, Ganbavle V V, Rajpure K Y. ZnO based visible-blind UV photodetector by spray pyrolysis. Superlattices Microstruct, 2014, 76, 253

[26] Shaikh S K, Inamdar S I, Ganbavle V V, et al. Chemical bath deposited ZnO thin film based UV photoconductive detector. J Alloys Compd, 2016, 664, 242

[27] Gurakar S, Serin T, Serin N. Electrical and microstructural properties of (Cu, Al, In)-doped SnO_2 films deposited by spray pyrolysis. Adv Mater Lett, 2014, 5, 309

[28] Lekshmy S S, Daniel G P, Joy K. Microstructure and physical proper-

ties of sol gel derived SnO_2: Sb thin films for optoelectronic applications. Appl Surf Sci, 2013, 274, 95

[29] Djamil R, Aicha K, Souifi A, et al. Effect of annealing time on the performance of tin oxide thin films ultraviolet photodetectors. Thin Solid Films, 2017, 623, 1

[30] Bhorde A, Waykar R, Nair S, et al. Room temperature synthesis of transparent and conducting indium tin oxide films with high mobility and figure of merit by RF-magnetron sputtering. J Electron Mater, 2019, 48, 7192

[31] He L N, Cao Q, Feng X J, et al. Structural, optical and electrical properties of epitaxial rutile SnO_2 films grown on MgF_2 (110) substrates by MOCVD. Ceram Int, 2018, 44, 869

[32] Abdelkrim A, Rahmane S, Ouahab Abdelouahab O, et al. Effect of solution concentration on the structural, optical and electrical properties of SnO_2 thin films prepared by spray pyrolysis. Optik, 2016, 127, 2653

[33] Al-Jawad S M H. Influence of multilayer deposition on characteristics of nanocrystalline SnO_2 thin films produce by Sol-gel technique for gas sensor application. Optik, 2017, 146, 17

[34] Ammar A H, Abo-Ghazala M S, Farag A A M, et al. Effect of gas type, pressure and temperature on the electrical characteristics of Al-doped SnO_2 thin films deposited by RGTO method for gas sensor application. Vacuum, 2013, 94, 30

[35] Chen H, Liu D T, Wang Y F, et al. Enhanced performance of planar perovskite solar cells using low-temperature solution-processed Al-doped SnO_2 as electron transport layers. Nanoscale Res Lett, 2017, 12, 238

[36] Bouznit Y, Henni A. Characterization of Sb doped SnO_2 films prepared by spray technique and their application to photocurrent generation. Mater Chem Phys, 2019, 233, 242

[37] Zhelev V, Petkov P, P. Shindov P, et al As-doped SnO_2 thin films for use as large area position sensitive photodetector. Thin Solid Films, 2018, 653, 19

[38] Aldemir D A, Benhaliliba M, Benouis C E, et al. Photodiode based on Al-doped SnO_2: Fabrication, current-voltage and capacitance-conductance-voltage measurements. Optik, 2020, 222, 165487

[39] Marimuthu G, Saravanakumar K, Jeyadheepan K, et al. Influence of twin boundaries on the photocurrent decay of nanobranch and dense-forest structured SnO_2 UV photodetectors. Superlattices Microstruct, 2019, 128, 181

[40] Wu J J, Huang Q W, Zeng D W, et al. Al-doping induced formation of oxygen-vacancy for enhancing gas-sensing properties of SnO_2 NTs by electrospinning. Sens Actuat B, 2014, 198, 62

[41] Ahmed S F, Ghosh P K, Khan S, et al. Low-macroscopic field emission from nanocrystalline Al doped SnO_2 thin films synthesized by Sol-gel technique. Appl Phys A, 2007, 86, 139

[42] Rahal A, Benhaoua A, Bouzidi C, et al. Effect of antimony doping on the structural, optical and electrical properties of SnO_2 thin films prepared by spray ultrasonic. Superlattices Microstruct, 2014, 76, 105

[43] Sinha S K, Ray S K, Manna I. Effect of Al doping on structural, optical and electrical properties of SnO_2 thin films synthesized by pulsed laser deposition. Philos Mag, 2014, 94, 3507

[44] Soumya S S, Vinodkumar R, Unnikrishnan N V. Conductivity type inversion and optical properties of aluminium doped SnO_2 thin films prepared by sol-gel spin coating technique. J Sol-Gel Sci Technol, 2021, 99, 636

[45] Sujatha K, Seethalakshmi T, Sudha A P, et al. Photocatalytic activity of pure, Zn doped and surfactants assisted Zn doped SnO_2 nanoparticles for degradation of cationic dye. Nano Struct Nano Objects, 2019, 18, 100305

[46] El Sayed A M, Taha S, Shaban M, et al. Tuning the structural, electrical and optical properties of tin oxide thin films via cobalt doping and annealing. Superlattices Microstruct, 2016, 95, 1

[47] Sivakumar P, Akkera H S, Reddy T R K, et al. Effect of Ti doping on structural, optical and electrical properties of SnO_2 transparent conducting thin films deposited by sol-gel spin coating. Opt Mater, 2021, 113, 110845

[48] Lin Z D, Li N, Chen Z, et al. The effect of Ni doping concentration on the gas sensing properties of Ni doped SnO_2. Sens Actuat B, 2017, 239, 501

[49] Korotkov R Y, Ricou P, Farran A J E. Preferred orientations in polycrystalline SnO_2 films grown by atmospheric pressure chemical vapor deposition. Thin Solid Films, 2006, 502, 79

[50] Kim C Y, Riu D H. Texture control of fluorine-doped tin oxide thin film. Thin Solid Films, 2011, 519, 3081

[51] Wang J T, Shi X L, Zhong X H, et al. Morphology control of fluorine-doped tin oxide thin films for enhanced light trapping. Sol Energy Mater Sol Cells, 2015, 132, 578

[52] Teldja B, Noureddine B, Azzeddine B, et al. Effect of indium doping on the UV photoluminescence emission, structural, electrical and optical properties of spin-coating deposited SnO_2 thin films. Optik, 2020, 209, 164586

[53] Reddy N N K, Akkera H S, Sekhar M C, et al. Zr-doped SnO_2 thin films synthesized by spray pyrolysis technique for barrier layers in solar cells. Appl Phys A, 2017, 123, 761

[54] Yang Y Z, Zhou W, Liang Y H, et al. Tuning band gap and ferromagnetism in epitaxial Al-doped SnO_2 films by defect engineering. J Cryst Growth, 2015, 430, 75

[55] Baig F, Ashraf M W, Asif A, et al. A comparative analysis for effects of solvents on optical properties of Mg doped ZnO thin films for optoelectronic applications. Optik, 2020, 208, 164534

[56] Bagheri-Mohagheghi M M, Shokooh-Saremi M. The influence of Al doping on the electrical, optical and structural properties of SnO_2 transparent conducting films deposited by the spray pyrolysis technique. J Phys D, 2004, 37, 1248

[57] Benouis C E, Benhaliliba M, Z. Mouffak Z, et al The low resistive and transparent Al-doped SnO_2 films: P-type conductivity, nanostructures and photoluminescence. J Alloys Compd, 2014, 603, 213

[58] Smith R W, Rose A. Space-charge-limited Currents in single crystals of cadmium sulfide. Phys Rev, 1955, 97, 1531

[59] Mishra S K, Srivastava R K, Prakash S G. ZnO nanoparticles: Structural, optical and photoconductivity characteristics. J Alloys Compd, 2012, 539, 1

[60] Shankar R, Srivastava R K. Photoconductivity and luminescence properties of gadolinium doped zinc oxide. Proc Natl Acad Sci, India, Sect A Phys Sci, 2018, 88, 137

[61] Farooqi M M H, Srivastava R K. Effect of annealing temperature on structural, photoluminescence and photoconductivity properties of ZnO thin film deposited on glass substrate by sol-gel spin coating method. Proc Natl Acad Sci India Sect A Phys Sci, 2020, 90, 845

[62] Agrahari V, Mathpal M C, Kumar M, et al. Investigations of optoelectronic properties in DMS SnO_2 nanoparticles. J Alloys Compd, 2015, 622, 48

[63] Kim D, Leem J Y. Morphology changes of In-doped ZnO nanosheets via $ZnCl_2$ and $InCl_3$ vapor formation during thermal dissipation annealing process and improved UV photoresponse properties. J Alloys Compd, 2021, 877, 160241

[64] Kim J M, Lim S J, Nam T, et al. The effects of ultraviolet exposure on the device characteristics of atomic layer deposited-ZnO:N thin film transistors. J Electrochem Soc, 2011, 158, J150

[65] Yang T T, Sun B, Ni L, et al. The mechanism of photocurrent enhancement of ZnO ultraviolet photodetector by reduced graphene oxide. Curr Appl Phys, 2018, 18, 859

[66] Zhou W Q, Yao G Y, Chen L J, et al. Pretreatment hematocrit is negatively associated with response to neoadjuvant chemotherapy in breast cancer. Biomark Med, 2017, 11, 713

[67] Gröttrup J, Postica V, Smazna D, et al. UV detection properties of hybrid ZnO tetrapod 3-D networks. Vacuum, 2017, 146, 492

[68] Kumar N, Srivastava A. Green photoluminescence and photocon-

ductivity from screen-printed Mg doped ZnO films. J Alloys Compd, 2018, 735, 312
[69] Ghosh T, Basak D. Highly enhanced ultraviolet photoresponse property in Cu-doped and Cu-Li co-doped ZnO films. J Phys D, 2009, 42, 145304
[70] Rose A. Space-charge-limited Currents in solids. Phys Rev, 1955, 97, 1538
[71] Randall J T, Wilkins M H F. Phosphorescence and electron traps - I. The study of trap distributions. Proc R Soc Lond A, 1945, 184, 365
[72] Gupta A, Verma N K, Bhatti H S. Fast photoluminescence decay processes of doped ZnO phosphors. Appl Phys B, 2007, 87, 311
[73] Agrahari V, Tripathi A K, Mathpal M C, et al. Effect of Mn doping on structural, optical and magnetic properties of SnO_2 nanoparticles. J Mater Sci: Mater Electron, 2015, 26, 9571
[74] Kong J T, Zheng W, Liu Y S, et al. Persistent luminescence from Eu^{3+} in SnO_2 nanoparticles. Nanoscale, 2015, 7, 11048

Kaour Selma received graduate degrees and Master's degree in physics from Guelma University, Algeria in 2013 and 2015 respectively. Now she is a PhD student in Oum El Bouaghi University. Her research interests on thin films synthesis by sol-gel and co-precipitation method and study their optical, electrical and photoconductivity properties.

Benkara Salima received the graduate engineering, Master and Doctorate of Science on Materials and components and components in electronics from Constantine University, Algeria, in 1997, 2000 and 2014 respectively. She is presently a teacher in Oum El Bouaghi University, Algeria. Her research interests on nanostructured films based on SnO_2, ZnO, and TiO_2.